Proceedings of the
Annual Stability Conference
Structural Stability Research Council
Atlanta, Georgia, April 21-24, 2026

O.I.C.-based design of hot-rolled steel channel sections under compression

Morane C. M. Wack[1], Oudom Chhoeng[2], Nicolas Boissonnade[3], Robert Tremblay[4]

Abstract
This paper investigates the ultimate compressive resistance of hot-rolled steel channel sections. Based on shell finite element models validated against experimental data, non-linear numerical analyses were conducted to assess the influence of a wide a range of cross-section geometries, local slenderness, and material properties on the cross-sectional resistance of channel sections. Consequently, numerical and experimental results were compared with current design standards. The findings indicate that European provisions tend to yield conservative predictions, while the American Specification often underestimates the effects of local buckling, leading to unconservative results and potential safety concerns. To overcome these limitations, an advanced design approach based on the Overall Interaction Concept (O.I.C.) is proposed, providing more accurate, consistent, and reliable predictions of the compressive strength of hot-rolled steel channel sections.

1. Introduction

Advances in manufacturing processes have enabled the use of high-strength structural steels, leading to an increased adoption of thin-walled members, including hot-rolled open sections. While the incorporation of slender plate elements improves structural efficiency by reducing self-weight and fabrication costs, it also increases the susceptibility of such sections to instability. Among open cross-sections, channel sections occupy a distinctive position, particularly for structural support, bracing, reinforcement and as main components of built-up members. Their mono-symmetry, combined with the presence of slender webs and flanges, makes their local buckling response particularly sensitive to plate interaction and stress redistribution effects.

In current design practice, local buckling effects in thin-walled members are predominantly addressed through the Effective Width Method (E.W.M.), which originates from isolated plate buckling theory (Von Kármán 1932, Winter 1947). In this approach, the resistance of a slender cross-section is evaluated by replacing each plate element with a reduced effective width, derived assuming idealized boundary conditions and uniform stress distributions. Although this methodology has been widely adopted due to its simplicity and clear mechanical background, it

[1] PhD Candidate, Polytechnique Montreal, <morane-chloe.mefande-wack@etud.polymtl.ca>
[2] PhD Candidate, Polytechnique Montreal, <oudom.chhoeng@etud.polymtl.ca>
[3] Professor, Laval University, <nicolas.boissonnade@gci.ulaval.ca>
[4] Professor, Polytechnique Montreal, <robert.tremblay@polymtl.ca>

focuses on plate elements independently and does not explicitly account for the interaction between adjacent plates within a cross-section. Experimental and numerical evidence has demonstrated that such isolated-plate assumptions are not fully representative of the actual local buckling behavior. The web-flange junction provides partial rotational restraint, while the free edges of the flanges remain unrestrained, leading to boundary conditions that differ from the classical simply supported or fully fixed cases assumed in plate theory (Kato 1985, Seif and Schafer 2010). As a result, the local buckling behavior, the post-buckling response, and the redistribution of stresses within the cross-section are governed by the combined response of the web and flanges rather than by the behavior of individual plates.

Further limitations of the E.W.M. arise from its treatment of post-buckling behavior. By replacing complex non-uniform stress fields with an equivalent uniform stress acting over a fictitious effective width, the method does not explicitly capture the redistribution of stresses that develops after local buckling. Experimental studies on welded H- and channel sections (Kwon et al. 2007) as well as on I- and channel sections (Rusch and Lindner 2001) have shown that this simplification may lead to overly conservative predictions of the cross-sectional resistance, particularly for slender open sections where plate interaction and membrane action are significant. These observations indicate that local buckling in channel sections is inherently a section-level phenomenon and cannot be fully described by plate-by-plate reduction rules.

To provide a more consistent representation of instability phenomena, the Overall Interaction Concept (O.I.C.), a slenderness-based design method has been proposed in which member buckling curves are expressed through non-dimensional $\chi - \lambda$ relationships derived from the extended Ayrton-Perry formula (Ayrton and Perry 1886). Within this context, the O.I.C. establishes a unified framework for describing buckling by defining reduction factors associated with distinct instability modes (Boissonnade et al. 2017). When restricted to cross-sectional behavior due to axial loading, this framework defines a local buckling reduction factor χ_L expressed as a function of a local relative slenderness λ_L. Both parameters are defined in Eq. (1) where N_{pl} is the the full plastic capacity of the cross-section under compression, $N_{cr,L}$ is the local elastic critical buckling load, $N_{u,L}$ is the local ultimate resistance. Further details are provided in Section 2.

$$\begin{cases} \lambda_L = \sqrt{N_{pl} / N_{cr,L}} \\ \chi_L = N_{u,L} / N_{pl} \end{cases} \tag{1}$$

This formulation provides a rational basis for treating local buckling independently of member-behavior while consistently accounting for imperfections, plate interaction and post-buckling strength reserves (Li et al. 2022). The present paper adopts this conceptual basis and focuses exclusively on the local buckling resistance of hot-rolled channel sections under axial compression. Global buckling and member-level instability effects are intentionally excluded to isolate cross-sectional behavior. Finite element (F.E.) analyses are used to determine the local reduction factor χ_L for a wide range of channel geometries, accounting for realistic plate interaction, geometric imperfections and material nonlinearity. On this basis, O.I.C.-based design equations are proposed, and their predictions are assessed against existing design provisions.

2. Design provisions for axially loaded members and the Overall Interaction Concept (O.I.C.)

2.1 Design provisions of the American Specifications (American Institute of Steel Construction 2022)

According to the American Specification for Structural Steel Buildings (A.I.S.C.), for compression members, the design strength is obtained by multiplying the nominal strength P_n by the resistance factor ϕ_c (taken as 0.9). For non-slender sections, the nominal strength depends on the governing buckling mode and is given by:

$$P_n = F_n \cdot A \tag{2}$$

In this expression, A is the gross cross-sectional area and F_n is the nominal stress hereby taken as the yield strength, F_y, for the calculation of the cross-sectional resistance. For members with slender sections, A.I.S.C. adopts the effective area method, in which the gross cross-sectional area A is replaced by an effective area A_e obtained from effective plate widths, determined as follows:

$$\begin{cases} b_e = b & \text{for } \dfrac{b}{t} \le \lambda_r \sqrt{\dfrac{F_y}{F_n}} \\ b_e = b\left(1 - c_1 \sqrt{\dfrac{F_{el}}{F_n}}\right)\sqrt{\dfrac{F_{el}}{F_n}} & \text{for } \dfrac{b}{t} > \lambda_r \sqrt{\dfrac{F_y}{F_n}} \end{cases} \tag{3}$$

In these expressions, λ_r represents the limiting width-to-thickness ratio of the plate, c_1 and c_2, the imperfection adjustment factors determined from Table E7.1 of A.I.S.C., and F_{el}, the elastic local buckling stress determined either numerically or analytically from Eq. (4). For channel sections, $c_1 = 0.22$ and $c_2 = 1.49$ for flanges, while $c_1 = 0.18$ and $c_2 = 1.31$ for the web plate of theses sections.

$$F_{el} = \left(c_2 \frac{\lambda_r}{(b/t)}\right)^2 F_y \tag{4}$$

The effective cross-sectional area is subsequently obtained by deducting from A the ineffective portions of each plate element, as described in Eq. (5).

$$A_e = A - \sum (b - b_e) t \tag{5}$$

2.2 Design provisions of the European Standard (European Committee for Standardization 2018)

The European Standard for steel structures, Eurocode 3 (EC3), adopts a classification for sections under compression from Class 1 (compact) to Class 4 (slender). For Class 1 to 3 cross-sections, EC3 defines the ultimate cross-sectional resistance for compression members as the full plastic capacity $N_{pl} = A \cdot F_y$. A partial safety factor $\gamma_{M0} = 1.00$ is applied for compression members to obtain the design value of the resistance. For Class 4 cross-sections, local buckling effects are accounted for by replacing the gross area, A, by the effective area A_e in the evaluation of the cross-sectional resistance.

For Class 4 plate elements in compression, Eurocode 3 (EC3) Part 1-5 on plated structures (European Committee for Standardization 2006) – referred to as EN 1993-1-5 – defines the effective area of each plate using Eq. (6), where ρ is the reduction factor for plate buckling.

$$A_e = \rho \cdot A \tag{6}$$

Flanges are modelled as outstand elements, stiffened along one longitudinal edge and free along the other, whereas webs are treated as internal elements stiffened along both longitudinal edges. The corresponding reduction factors are given by Eq. (7).

$$\begin{cases} \begin{cases} \rho = 1.0 & \text{for } \bar{\lambda}_p \le 0.5 + \sqrt{0.085 - 0.055\psi} \\ \rho = \dfrac{\bar{\lambda}_p - 0.055(3+\psi)}{\bar{\lambda}_p^2} & \text{for } \bar{\lambda}_p > 0.5 + \sqrt{0.085 - 0.055\psi} \end{cases} & \text{for outstand compression elements} \\ \begin{cases} \rho = 1.0 & \text{for } \bar{\lambda}_p \le 0.748 \\ \rho = \dfrac{\bar{\lambda}_p - 0.188}{\bar{\lambda}_p^2} & \text{for } \bar{\lambda}_p > 0.748 \end{cases} & \text{for internal compression elements} \end{cases} \tag{7}$$

In these expressions, ψ is the ratio of longitudinal stresses at the plate edges, while $\bar{\lambda}_p$ represents the relative plate slenderness defined in Eq. (8) where k is the buckling factor corresponding to the stress ratio ψ and the plate boundary conditions.

$$\bar{\lambda}_p = \sqrt{\frac{F_y}{\sigma_{cr}}} = \sqrt{\frac{F_y}{\dfrac{\pi^2 E k}{12\left(1-\nu^2\right)\left(b/t\right)^2}}} \cong \frac{b/t}{28.4\varepsilon\sqrt{k}}, \text{ where: } \varepsilon = \sqrt{235 / F_y\,[MPa]} \tag{8}$$

2.3 The Overall Interaction Concept (O.I.C.)

The O.I.C. is based on the interaction between two fundamental phenomena, namely resistance and instability, as illustrated in Fig. 1 showing the O.I.C. design flow chart for local buckling.

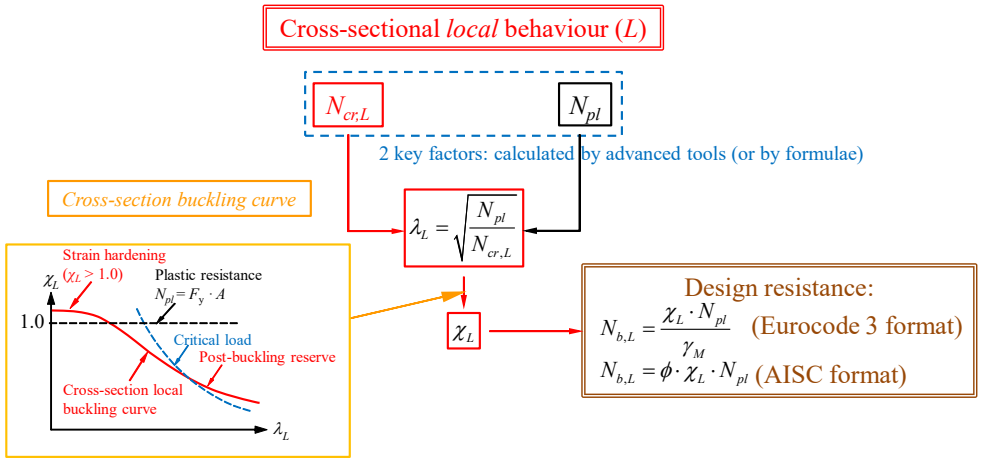

Figure 1: O.I.C. design flow chart for local buckling.

This design approach provides a unified and efficient framework for predicting the behavior and load-carrying capacity of structural members. A key advantage of the O.I.C. lies in its ability to avoid both cross-section classification and the use of the E.W.M. (Nseir 2015, Boissonnade et al. 2017, Li et al. 2022), which remains computationally demanding in practical applications. The approach is formulated in a dimensionless $\chi - \lambda$ format, where the reduction factor χ is expressed as a function of a generalized relative slenderness λ, defined in Eq. (1). As illustrated in Fig. 1, compact sections may exhibit χ_L values exceeding unity due to strain hardening, whereas slender sections or long members experience a progressive reduction in resistance governed by instability effects. The $\chi - \lambda$ format allows representing various buckling modes as well as a wide range of geometrical and material properties in a unified figure. It also provides a continuous and mechanically consistent description of structural behavior across a wide range of slenderness values.

Within the O.I.C., the buckling curves are formulated using the extended Ayrton-Perry formula defined by Eq. (9). In this formulation, α refers to the imperfection factor that is equal to 0.49 for channel sections in EC3, β to the resistance limit that might be affected by post-buckling reserves in the short slenderness range, δ to the instability limit that accounts for a possible variation in the instability limit, and λ_0 to the end-of-plateau limit that is equal to 0.2 in EC3.

$$\chi = \frac{\beta}{\phi + \sqrt{\phi^2 - \lambda^\delta}}$$
$$\phi = 0.5\left(1 + \alpha\left(\lambda - \lambda_0\right) + \lambda^\delta\right) \tag{9}$$

Based on this definition, the O.I.C. design procedure consists of the following steps:

- Determination of N_{pl}, corresponding to the plastic resistance limit;
- Determination of N_{cr}, corresponding to the instability limit;
- Evaluation of the generalized relative slenderness λ;
- Determination of the reduction factor $\chi = f(\lambda)$ from the buckling curve;
- Calculation of the ultimate resistance as $N_u = \chi \cdot N_{pl}$.

3. Numerical modelling

3.1 Development of the F.E. models

Numerical simulations were performed using the F.E. software Abaqus 2023 (Dassault Systèmes 2014) to investigate the local buckling behavior of hot-rolled channel sections under compression. Both Linear Buckling Analyses (L.B.A.) and displacement-controlled Geometric and Material Nonlinear Analyses with Imperfections (G.M.N.I.A.) were carried out. The members were modelled using four-node quadrilateral shell elements with reduced integration (S4R), which have been shown to accurately capture the elastic buckling and post-buckling response of thin-walled steel plates (Dassault Systèmes 2014).

A preliminary mesh sensitivity study was conducted to balance numerical accuracy and computational efficiency. Based on the results, a uniform mesh size equal to one tenth of the flange width, with unit aspect ratio (width/length = 1), was adopted for all models. Since the web-flange junctions of hot-rolled sections include fillet regions, which contributes to the torsional stiffness of the cross-section, an additional beam element (B31) was introduced along the centroidal axis of

the fillet region, with a cross-sectional area equivalent to that of the fillet, as illustrated in Fig. 2. In addition, linear spring elements arranged in a truss-like configuration were introduced at the position of the fillet area to mitigate unrealistic local buckling between adjacent plates while preserving realistic plate interaction. This modelling approach has been successfully employed in previous studies on open thin-walled sections (Li et al. 2022, Dahboul et al. 2023, Mefande Wack et al. 2025).

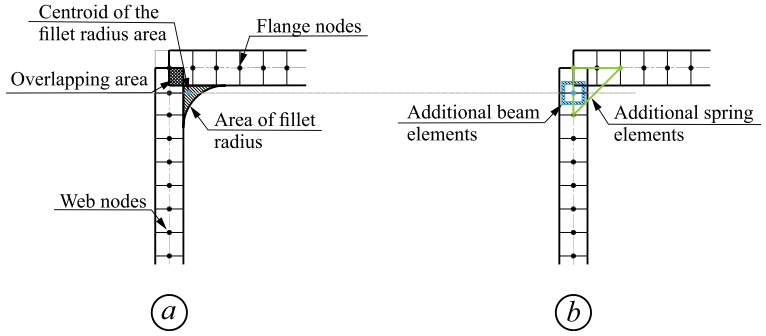

Figure 2: Modeling principles of hot-rolled channel sections: (a) Real geometry – (b) Modelled geometry.

Experimental boundary conditions were closely reproduced for the validation analyses, while fork-type support conditions were adopted for parametric studies, as illustrated in Fig. 3. Reference points (R.P.) were defined at the geometric centroids of the end sections and linked to the corresponding nodes using rigid body constraints, ensuring uniform load distributions to each node of the end sections. At both ends, torsional rotation and out-of-plane displacements were restrained. Axial displacements were allowed at the loaded end, while restrained at the other end. To accurately reproduce experimental support conditions, a longitudinal eccentricity (see e_z in Fig. 3) between the reference point and the end section was introduced in the validation analyses when, and global warping was restrained. In contrast, for parametric studies, idealized axial loading without eccentricity was adopted and warping was still restrained since only local buckling was observed.

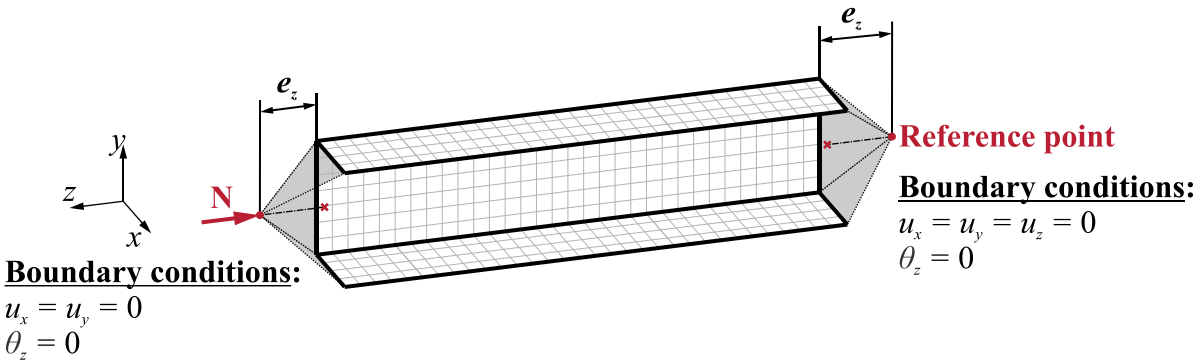

Figure 3: Fork-type support conditions for channel sections.

Material behavior was defined using the quad-linear stress-strain model proposed by Yun (2017) for parametric analyses, while experimentally measured stress-strain curves were used for model validation. In all cases, material properties were converted to true stresses and strains prior in numerical models.

In the absence of experimental data on residual stress distributions in hot-rolled channel sections, a self-equilibrated linear residual stress pattern was adopted, following the model proposed by Beyer (2017) illustrated in Fig. 4a defined with the parameter $\xi = 1 + b \cdot t_f / (h \cdot t_w)$, where b, t_f, t_w, and h denote the flange width, flange thickness, web height, and web thickness, respectively. Although direct measurements are not available, this residual stress model has been previously used in numerical investigations of hot-rolled steel members and satisfies equilibrium requirements (Lindner and Glitsch 2004, Snijder et al. 2008, Beyer 2017). Initial geometric imperfections were introduced using the sine-shaped distributions illustrated in Figs. 4b and 4c. This approach has been successfully applied in numerical studies on I-sections, hollow sections and channel sections (Gérard et al. 2019, Li et al. 2022, Mefande Wack et al. 2025).

Geometric imperfections only included local imperfections that were defined independently for the web and flanges based on their individual buckling lengths a_w and a_f (see Eq. (10)), respectively. The sine-shaped imperfection pattern was defined with a half-wavelength equal to the average buckling length, a_{avg} defined in Eq. (10) and an amplitude set to 1/200th of the corresponding plate buckling length, following the methodology proposed for hot-rolled channel sections (Mefande Wack et al. 2025).

$$\begin{aligned} a_f &= 2 \cdot (b - t_w - r) \\ a_w &= h - 2\,t_f - 2\,r \\ a_{avg} &= (a_f + a_w)/2 \end{aligned} \tag{10}$$

Therefore, a case denoted as "$HWL = a_{avg} \mid L = 3a_{avg} \mid Ampl. = a_{pp} / 200$" represents a member with a length of three half-waves, each with a wavelength equal to the average of the web and flange buckling lengths (a_w and a_f, respectively), and an amplitude of imperfection of 1/200th of the buckling length per plate a_{pp} (a_w for the web and a_f for the flanges).

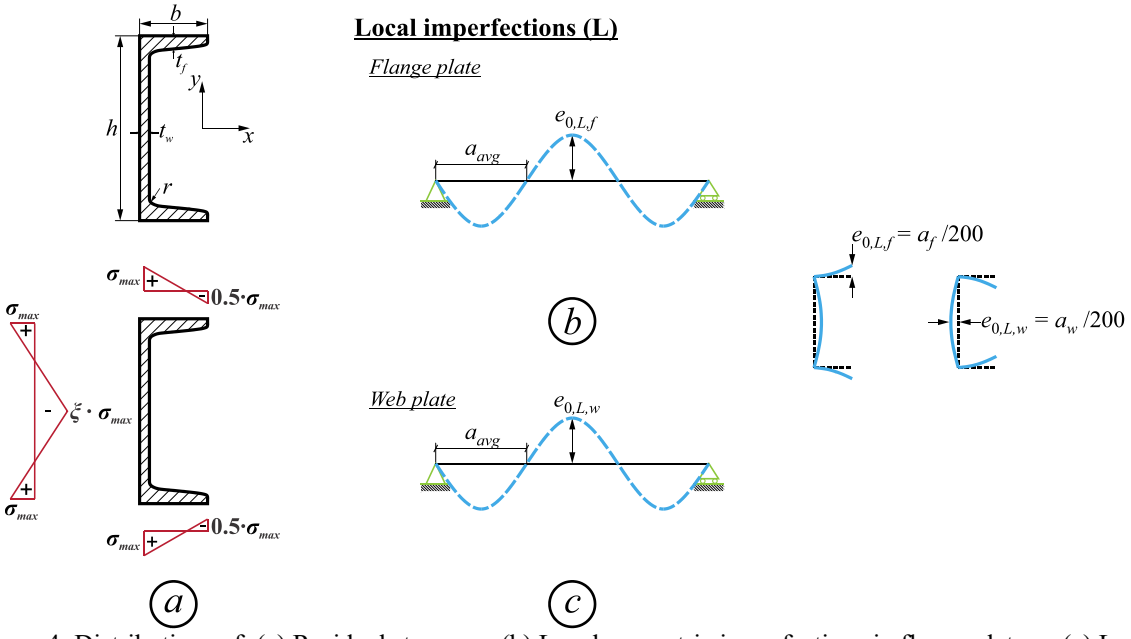

Figure 4: Distributions of: (a) Residual stresses – (b) Local geometric imperfections in flange plates – (c) Local geometric imperfections in web plates.

To ensure that the numerical response is governed solely by cross-sectional effects, a parametric validation procedure was performed with the aim to finding the appropriate length of the member to consider in the numerical models that is short enough so that any global behavior is prevented while remaining long enough to limit the effect of end supports on the ultimate resistance.

3.2 Validation of numerical models

Based on an extensive literature review, 16 stub column test results reported by Li (2023) were collected to compare different assumed initial geometric imperfection shapes with experimentally measured imperfections. The dataset comprises hot-rolled channel sections C80×40×5, C100×50×5, and C100×50×6, manufactured from EN 1.4301 austenitic stainless steel and tested under simple and combined loading conditions. Table 1 reports the key parameters of these tests and Fig. 5 presents a comparison between experimental cross-sectional resistances and their numerical counterparts. In Fig. 5, the vertical axis represents the ratio of the ultimate local resistance obtained from FE analyses, $N_{u,FE}$, to that obtained experimentally, $N_{u,Exp}$. The horizontal axis specifies the specimen designations along with their respective load types.

The validation process involved members with a length corresponding to three halfwaves as suggested by a previous study on the local behavior of channel section (Mefande Wack et al. 2025), corresponding to the case $HWL = a_{avg} \mid L = 3a_{avg} \mid Ampl. = a_{pp} / 200$. An additional case was considered were the actual length, L_0, the measured amplitude of local imperfections, e_0, and a half-wavelength of a_{avg} were used, and was denoted as $HWL = a_{avg} \mid L = L_0 \mid Ampl. = e_0$.

Table 1: Test data and corresponding sine shapes periods and amplitudes.

ID	Load type	b (mm)	h (mm)	t (mm)	r (mm)	L_0 (mm)	e_0 (mm)	a_f (mm)	a_w (mm)	a_{avg} (mm)	$a_f/200$ (mm)	$a_w/200$ (mm)
C1-S1	N	39.75	80.46	4.79	4.74	178.2	0.03	60.44	61.40	60.92	0.30	0.31
C1-S2	N	39.8	80.39	4.72	4.75	178.3	0.05	60.66	61.45	61.06	0.30	0.31
C2-S1	N	49.75	98.91	4.8	4.84	225.8	0.04	80.22	79.63	79.93	0.40	0.40
C2-S2	N	49.69	98.93	4.72	4.76	219	0.04	80.42	79.97	80.20	0.40	0.40
C3-S1	N	49.15	100.11	5.62	5.61	224.2	0.06	75.84	77.65	76.75	0.38	0.39
C3-S2	N	49.18	100.16	5.72	5.74	224.4	0.05	75.44	77.24	76.34	0.38	0.39
C1	N + M_y	49.65	98.93	4.82	4.91	375.2	0.03	79.84	79.47	79.66	0.40	0.40
C2	N + M_y	49.62	98.99	4.79	4.85	372.9	0.04	79.96	79.71	79.84	0.40	0.40
C3	N + M_y	49.62	98.99	4.79	4.87	372.9	0.04	79.92	79.67	79.80	0.40	0.40
C4	N + M_y	49.75	98.95	4.77	4.9	373.8	0.04	80.16	79.61	79.89	0.40	0.40
C5	N + M_y	49.61	98.97	4.73	4.63	373.0	0.04	80.5	80.25	80.38	0.40	0.40
RC1	N + M_y	49.74	99.05	4.86	4.77	373.5	0.03	80.22	79.79	80.01	0.40	0.40
RC2	N + M_y	50.27	99.01	4.79	4.94	373.8	0.04	81.08	79.55	80.32	0.41	0.40
RC3	N + M_y	49.59	98.97	4.75	4.85	373.7	0.03	79.98	79.77	79.88	0.40	0.40
RC4	N + M_y	49.79	98.91	4.71	4.66	373.2	0.04	80.84	80.17	80.51	0.40	0.40
RC5	N + M_y	49.65	98.91	4.76	4.64	371.6	0.03	80.5	80.11	80.31	0.40	0.40

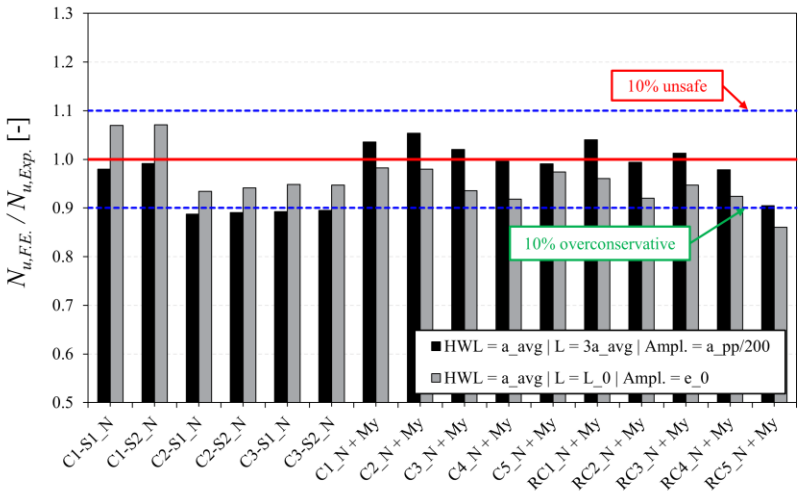

Figure 5: Comparison of experimental tests with F.E. results.

Figure 5 shows a good agreement between the experimental results and the numerical simulations when geometric imperfections are defined using either the measured specimen length and maximum imperfection amplitude ($HWL = a_{avg} \mid L = L_0 \mid Ampl. = e_0$) or a sine-shaped imperfection with an amplitude equal to a_{pp} / 200 ($HWL = a_{avg} \mid L = 3a_{avg} \mid Ampl. = a_{pp} / 200$). For the latter case, the mean value of the ratio $N_{u,FE} / N_{u,Exp}$ is 0.97 with a Coefficient of Variation (C.o.V.) of 5.8%, while corresponding values of 0.96 and 5.3% are obtained for $HWL = a_{avg} \mid L = L_0 \mid Ampl. = e_0$. For most specimens, the FE-to-test ultimate capacity ratios remain close to unity, with deviations generally within ±10%. Slight overestimations observed in a limited number of combined-loading tests remain below 8% and are attributed to uncertainties in the applied loading eccentricities. For both configurations, the numerical load-displacement curves for specimen C1-S1 (Fig. 6a) show good agreement with the experimental response, and the corresponding failure modes at peak load are consistent with experimental observations (Fig. 6b).

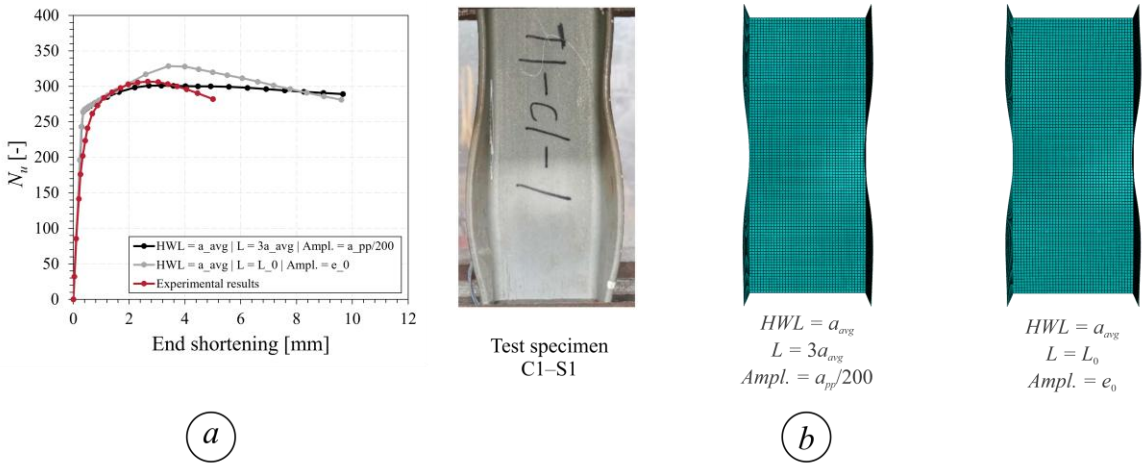

Figure 6: Results for specimen C1-S1: (a) Load-displacement curves – (b) Failure mode for .

Based on these observations, $HWL = a_{avg} \mid L = 3a_{avg} \mid Ampl. = a_{pp} / 200$ is adopted for the subsequent parametric studies, as it provides an accurate yet slightly conservative prediction of the

ultimate resistance, reproduces the measured load-displacement behavior, and offers a simple and reproducible imperfection definition suitable for systematic numerical investigations.

3.3 Selection of parameters

Once the F.E. modelling procedure was fully established, a comprehensive parametric study was carried out covering a broad spectrum of channel section geometries. The analyzed cross-sections comprised both slender and non-slender sections. In total, 300 hot-rolled channel cross-sections were considered. These sections were selected from standard steel catalogues and complemented by additional geometries to reflect typical constructional detailing encountered in practice.

Each case included both L.B.A. and G.M.N.I.A. analyses, with results expressed in the form of $\chi - \lambda$ curves. The studied section heights, h, ranged from 76.2 to 800 mm; flange widths, b, from 35.8 to 254 mm; flange thicknesses, t_f, from 5 to 18 mm; and web thicknesses, t_w, from 3 to 21.2 mm. Consequently, height-to-width ratios, h / b, ranged from 1.5 to 10.1; flange slenderness, b / t_f, from 5.0 to 20.8; and web slenderness, h / t_w, from 8.0 to 124. For each cross-section, three steel grades were considered: C.S.A. G40.4 (F_y = 230 MPa); C.S.A. G40.21 350W (F_y = 350 MPa) and C.S.A. G40.21 550W (F_y = 550 MPa). In total, 1 800 non-linear F.E. analyses, comprising 900 L.B.A. and 900 G.M.N.I.A., were performed.

4. O.I.C.-based design proposal

The local buckling design curve shown in Fig. 7 was derived from the extensive parametric study described in Section 3. The numerical results are presented in the $\chi - \lambda$ format, which facilitates the identification of the key parameters governing the cross-sectional response of hot-rolled channel sections in compression within the O.I.C. framework, based on the extended Ayrton-Perry formulation introduced in Eq. (9). The proposed local buckling curve incorporates two reference limits: (i) an upper bound corresponding to the full plastic resistance, defined by a reduction factor χ_L = 1.0 and indicated by a short-dashed grey line (resistance limit); and (ii) a stability limit represented by the Von Kármán curve for ideal thin plates without imperfections, $\chi_L = 1/\lambda_L$, shown as a long-dashed grey line.

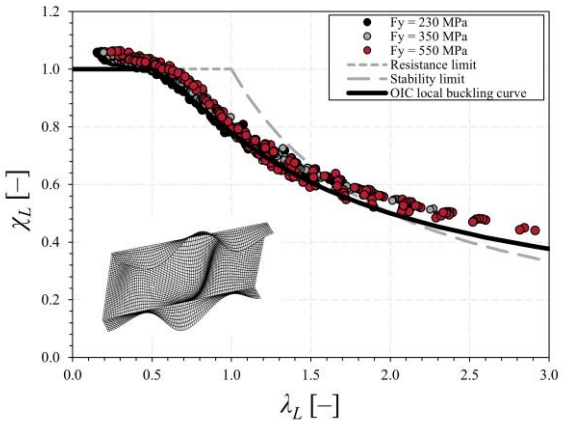

Figure 7: Influence of steel grades on ultimate cross-sectional resistance and O.I.C. buckling curve.

As shown in Fig. 7, the numerical results exhibit only a limited sensitivity to yield strength. Across the investigated steel grades (230 MPa to 550 MPa), the maximum variation in the local buckling response remains within approximately 5%, indicating that material strength effects are adequately

captured by the $\chi - \lambda$ format. This observation supports the use of a single local buckling curve to represent the local behavior of hot-rolled channel sections over a wide range of steel grades.

For non-slender sections with local slenderness $\lambda_L \leq 0.50$, the F.E. analyses yield reduction factors exceeding unity. This response is attributed to strain-hardening effects, which allow stresses to surpass the nominal yield strength at high strain levels. Such behavior is typical of compact cross-sections, which are less sensitive to local instability and can develop significant plastic deformation prior to failure. With increasing local slenderness, often associated with larger height-to-width ratios or increased plate width-to-thickness ratios, the predicted resistance decreases. This trend reflects the growing susceptibility of slender web and flange plates to local buckling, the reduced restraint provided by narrow flanges, and the progressive reduction of the effective load-carrying portion of the cross-section, which introduces secondary bending effects due to the eccentricity between the gross and (fictious) effective centroids.

For highly slender cross-sections ($\lambda_L \geq 1.50$), the numerically obtained reduction factors may exceed the idealized stability limit ($\chi_L = 1/\lambda_L$), as illustrated in Fig. 7. This behavior results from post-buckling strength reserves and the beneficial interaction between the web and flange plates, which provide additional stiffness beyond the theoretical elastic local buckling load. Table 2 summarizes the O.I.C.-based design equations for local buckling, expressed using the extended Ayrton-Perry formulation (see Eq. (9)). The assessment of this design proposal is presented in the following Section.

Table 2: Key parameters for local buckling curves of hot-rolled channel sections.

	α	β	δ	λ_0
Key parameters	0.125	1.0	0.70	0.50

5. Assessment of design proposal

A comparative study was conducted between F.E. results and analytical predictions of the cross-sectional resistances of channel sections. The analytical approaches considered include A.I.S.C. and EC3 detailed in Section 2 and the proposed O.I.C.-based formulation. The comparison is presented in Fig. 8 and Table 3 through the ratios $\chi_{L,\,Ref.} / \chi_{L,\,F.E.}$, plotted as functions of the local slenderness λ_L. Values exceeding unity indicate unconservative predictions, while ratios below unity represent conservative estimates.

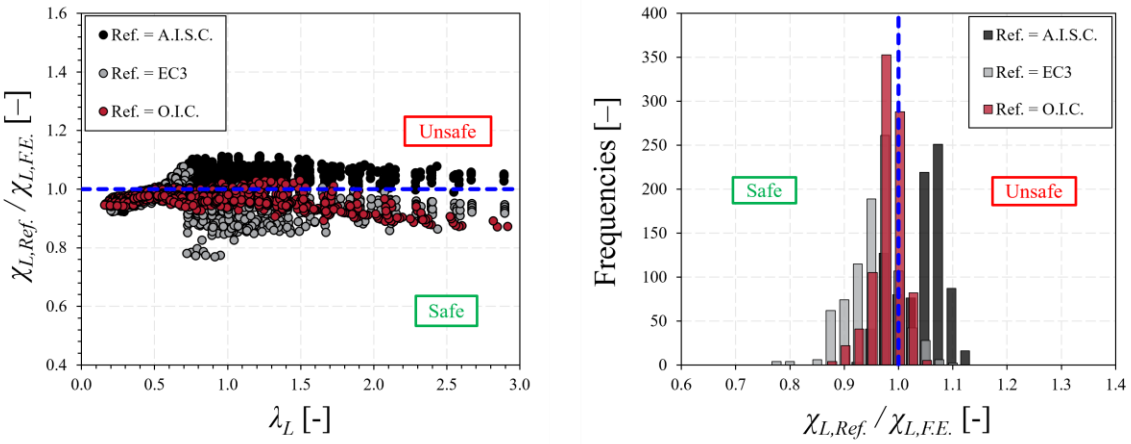

Figure 8: Analytical vs. F.E. results for hot-rolled channel sections in compression: (a) accuracy of cross-sectional resistance predictions – (b) cumulative frequencies distributions.

Table 3: Statistical results for $\chi_{L,Ref.} / \chi_{L,F.E.}$ ratios.

	Number of cases	Ref.	Mean	C.o.V. [%]	Max.	Min.	<0.90 [%]	>1.05 [%]	>1.10 [%]	>1.20 [%]
All F_y	900	O.I.C.	0.97	2.8	1.03	0.87	2.9	0.0	0.0	0.0
		A.I.S.C.	1.03	4.2	1.11	0.92	0.0	39.3	1.8	0.0
		EC3	0.94	4.8	1.08	0.77	16.7	0.9	0.0	0.0
F_y = 230 MPa	300	O.I.C.	0.98	1.9	1.02	0.91	0.0	0.0	0.0	0.0
		A.I.S.C.	1.04	4.5	1.11	0.94	0.0	46.7	5.3	0.0
		EC3	0.97	3.9	1.08	0.85	3.3	2.7	0.0	0.0
F_y = 350 MPa	300	O.I.C.	0.97	2.4	1.03	0.89	2.0	0.0	0.0	0.0
		A.I.S.C.	1.02	4.3	1.08	0.92	0.0	25.3	0.0	0.0
		EC3	0.93	4.2	1.05	0.78	20.7	0.0	0.0	0.0
F_y = 550 MPa	300	O.I.C.	0.96	3.4	1.03	0.87	6.7	0.3	0.0	0.0
		A.I.S.C.	1.03	3.7	1.08	0.94	0.0	68.3	0.0	0.0
		EC3	0.93	4.9	1.02	0.77	26.0	0.0	0.0	0.0

Using the O.I.C.-based approach as reference, the mean ratio $\chi_{L,\,O.I.C.} / \chi_{L,\,F.E.}$ is 0.97 with a low coefficient of variation (C.o.V.) of 2.8%, while the maximum unconservative deviation of 3%. As shown in Table 3, A.I.S.C. exhibits higher statistical accuracy, with a mean ratio $\chi_{L,\,A.I.S.C.} / \chi_{L,\,F.E.}$ of 1.03 and a C.o.V. of 4.2%, but tends to produce unconservative estimates, with more than 40% of predictions exceeding 5% of non-conservatism. EC3 predominantly yields conservative predictions, with a mean ratio of 0.94 and a C.o.V. of 4.8%, although minor unconservative deviations (up to about 8%) occur for moderately slender sections ($0.50 \leq \lambda_L \leq 0.75$).

Both A.I.S.C. and EC3 account for local buckling through effective cross-sectional properties derived from plate width-to-thickness limits. For hot-rolled channel sections with F_y = 350 MPa, the maximum allowable width-to-thickness ratios to not being considered slender for webs and flanges are 35.62 and 13.39 for A.I.S.C.; and 34.41 and 11.47 for EC3. Consequently, A.I.S.C. might predict larger effective areas and ultimate resistances, while the EC3 might yield lower estimates. A study of the influence of yield strength indicates that both EC3 and A.I.S.C. perform well for F_y = 230 MPa. At higher strength levels, EC3 becomes increasingly conservative, whereas the O.I.C.-based formulation maintains consistent accuracy. The remaining discrepancies in Standards provisions are attributed to the simplified treatment of plate interaction and boundary conditions inherent to the E.W.M., whereas the O.I.C. formulation, by treating the cross-section as a whole unit, provides more reliable and consistent predictions of cross-sectional resistances.

6. Conclusions

This paper presented a numerical investigation of the local buckling behavior of hot-rolled channel sections subjected to axial compression. Finite element models were developed and validated against available experimental data, demonstrating their ability to accurately reproduce cross-sectional buckling responses and post-buckling behavior. An extensive parametric study was subsequently conducted to examine the influence of cross-sectional geometry and material properties on cross-sectional resistance. The results showed that, although higher steel grades may exhibit increased nominal resistance due to strain hardening, the overall influence of yield strength on the local buckling response remains limited. Based on these findings, a single local buckling curve and a design formulation based on the Overall Interaction Concept were proposed using a unified $\chi - \lambda$ format. The proposed formulation provides a consistent and practical representation of the local buckling behavior of hot-rolled channel sections and demonstrates improved accuracy and consistency compared with existing effective-width-based provisions. Therefore, it offers a

rational and economical alternative for the design of hot-rolled channel sections submitted to compressive loads.

Acknowledgments
This research and development project would not have been possible without the contribution and collaboration of The Jacques Cartier and Champlain Bridges Incorporated.

References

American Institute of Steel Construction. (2022). *ANSI/A.I.S.C. 360-22: Specification for Structural Steel Buildings*.
Ayrton, W. E., & Perry, J. (1886). On struts. *The Engineer*, *62*.
Beyer, A. (2017). *On the Design of Members with Open Cross Sections Subject to Combined Axial Compression, Bending and Torsion* [PhD thesis]. Lorraine University.
Boissonnade, N., Hayeck, M., Saloumi, E., & Nseir, J. (2017). An Overall Interaction Concept for an alternative approach to steel members design. *Journal of Constructional Steel Research*, *135*, 199–212. https://doi.org/10/gbkrf8
Dahboul, S., Li, L., Coderre, T., & Boissonnade, N. (2023). O.I.C.-based design of extruded and welded aluminum I-sections. *Structures*, *58*, 105504. https://doi.org/10.1016/j.istruc.2023.105504
Dassault Systèmes Simulia Corp. (2014). *Getting Started with Abaqus: Interactive Edition*.
European Committee for Standardization (CEN). (2006). *EN 1993-1-5: Eurocode 3 – Design of steel structures – Part 1-5: Plated structural elements*. https://standards.globalspec.com/std/14500117/PREN%201993-1-5
European Committee for Standardization (CEN). (2018). *EN 1993-1-1: Eurocode 3 – Design of steel structures – Part 1-1: General rules and rules for buildings*. https://standards.globalspec.com/std/14327633/PREN%201993-1-1
Gérard, L., Li, L., Kettler, M., & Boissonnade, N. (2019). Recommendations on the geometrical imperfections definition for the resistance of I-sections. *Journal of Constructional Steel Research*, *162*, 105716. https://doi.org/10.1016/j.jcsr.2019.105716
Kato, B. (1989). Rotation capacity of H-section members as determined by local buckling. *Journal of Constructional Steel Research*, *13*(2–3), 95–109. https://doi.org/10/cs5bh3
Kwon, Y. B., Kim, N. G., & Hancock, G. J. (2007). Compression tests of welded section columns undergoing buckling interaction. *Journal of Constructional Steel Research*, *63*(12), 1590–1602. https://doi.org/10.1016/j.jcsr.2007.01.011
Li, L. (2021). *Extension of the Overall Interaction Concept to steel open sections and members* [PhD thesis]. Université Laval, Québec, Canada.
Li, L., Fafard, M., & Boissonnade, N. (2022). Local and global instabilities of rolled T-section columns under axial compression. *Thin-Walled Structures*, *178*, 109517. https://doi.org/10.1016/j.tws.2022.109517
Li, L., Gérard, L., Kettler, M., & Boissonnade, N. (2022). The Overall Interaction Concept for the design of hot-rolled and welded I-sections under combined loading. *Thin-Walled Structures*, *172*, 108623. https://doi.org/10.1016/j.tws.2021.108623
Li, S. (2023). *Behaviour and design of hot-rolled stainless steel channel section members* [PhD thesis]. Nanyang Technological University, Singapore.
Mefande Wack, M. C., Chhoeng, O., Tremblay, R., & Boissonnade, N. (2025). On the definition of geometric imperfections in the F.E. modelling of local buckling in hot-rolled channel sections. *Proceedings of the Annual Stability Conference Structural Stability Research Council, SSRC 2025*. Annual Stability Conference Structural Stability Research Council 2025, Louisville, KY, USA.
Nseir, J. (2015). *Development of a new design method for the cross-section capacity of steel hollow sections* [Université de Liège, Liège, Belgique]. https://orbi.ulg.ac.be/handle/2268/183084
Rusch, A., & Lindner, J. (2001). Remarks to the Direct Strength Method. *Thin-Walled Structures*, *39*(9), 807–820. https://doi.org/10/bswm6h
Seif, M., & Schafer, B. W. (2010). Local buckling of structural steel shapes. *Journal of Constructional Steel Research*, *66*(10), 1232–1247. https://doi.org/10/d8m64t
Von Kármán, T., Sechler, E. E., & Donnell, L. H. (1932). The Strength of Thin Plates in Compression. *Journal of Fluids Engineering*, *54*(2), 53–56. https://doi.org/10.1115/1.4021738
Winter, G. (1947). Strength of Thin Steel Compression Flanges. *Transactions of the American Society of Civil Engineers*, *112*(1), 527–554. https://doi.org/10.1061/TACEAT.0006092

Yun, X., & Gardner, L. (2017). Stress-strain curves for hot-rolled steels. *Journal of Constructional Steel Research*, *133*, 36–46. https://doi.org/10.1016/j.jcsr.2017.01.024